QUANTITATIVE NON-DESTRUCTIVE EVALUATION OF CRACK LENGTH AND STRESS INTENSITY FACTOR IN FATIGUED AUSTENITIC STAINLESS STEEL

Yuji Nakasone[1], Yoshifumi Iwasaki[1]

[1]Department of Mechanical Engineering, Tokyo University of Science, Tokyo, Japan

Abstract

The present study proposes a new non-destructive method not only for estimating length of fatigue cracks but for quantitatively evaluating maximum values of stress intensity factor applied to plate specimens of an austenitic stainless steel SUS304 (equivalent of AISI304) fatigued at room temperature. The method makes use of plasticity-induced martensitic phase transformation that takes place in the plasticity wake regions around growing fatigue cracks. Distributions of the volume fraction of α' martensitic phase around fatigue cracks were measured with ferrite scope. The results were compared with the distributions of strain measured by the digital image correlation method and with those of vertical magnetic flux density B_z above the fatigue cracks in plate specimens magnetized by a strong elctromagnet of 0.5 T. It was revealed that the distance between the points where B_z reached the maximum and minimum values B_{zmax} and B_{zmin} had good linear correlations with crack length 2*a* irrespective of the stress ratio *R*. The B_{zmax} and B_{zmin} values also showed good linear relations with the maximum values of the stress intensity factor K_{max} applied. The relations are also independent of the *R* ratio. These results imply that not only crack length but also maximum values of the applied stress intensity factor can be quantitatively evaluated in an electromagnetic non-destructive way.

1. Introduction

SUS 304 stainless steel (equivalent of AISI 304 stainless steel) is known as an austenitic stainless steel that has unstable γ austenitic phase around and below room temperature (RT). The stainless steel usually shows ductile and paramagnetic, or non-magnetic nature, whereas it becomes brittle and ferromagnetic even at RT under high stress or strain since the transformation of γ austenitic phase into α' martensitic phase can be enhanced in the steel by the application of stress or strain. The higher the stress or the strain becomes, the more the α' phase is induced by plasticity-induced transformation [1-4].

In past studies [5-7], the present authors measured the volume fraction $V_{\alpha'}$ of α' martensitic phase transformed in SUS 304 plate specimens subjected to uniform tensile stress at RT and at liquid nitrogen temperature with three types of equipments; i.e., vibrating sample magnetometer (VSM), X-ray diffractometer and ferrite scope in order to obtain the applied strain level dependence of $V_{\alpha'}$. The present study has attempted to establish the quantitative non-destructive inspection method for material degradation by using martensitic transformation.

2. Martensitic transformation at RT

In our past studies [5], tensile tests were made at RT in air to obtain relations between volume frac-

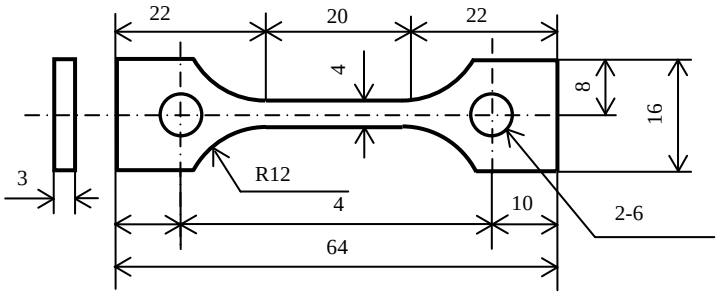

Figure 1*: Geometry of tensile specimens (unit: mm).*

Table 1: Chemical composition of SUS 304 stainless steel tested in this study (mass%).

Material	C	Si	Mn	P	S	Ni	Cr
SUS 304	0.06	0.50	0.87	0.037	0.01	8.1	18.21

tion $V_{\alpha'}$ of α' martensite transformed and the magnitude of strain applied. Figure 1 shows the geometry the tensile specimens used.

The chemical composition of SUS 304 steel used is shown in Table 1. In this study, three different types of measuring equipment, i.e., VSM, X-ray diffractometer and ferrite scope were used in obtaining the calibration diagrams for the measurement of the spatial distributions of $V_{\alpha'}$ around fatigue cracks with ferrite scope for the purpose of in-service inspection.

2.1. Methods of measuring α' volume fraction

In order to obtain martensitic volume fraction $V_{\alpha'}$ by VSM, the values of $V_{\alpha'}$ is determined via the ratios of the values of the saturation magnetization of deformed specimens to those of the fully transformed specimen of the present SUS304 steel. The $V_{\alpha'}$ value of the fully transformed SUS304 specimen can be calculated by the Slater-Pauling diagram (see [4], for example). The X-ray diffraction method was used for the quantitative analysis of γ austenitic and α' martensitic phases which have face-centered cubic (fcc) and body-centered tetragonal (bct) structures, respectively. In general X-ray quantitative analysis, the volume fraction of α' martensitic phase can be calculated from the ratio of integrated diffraction-intensity peaks for α' martensitic and γ austenitic phases. In the present study, however, since integrated intensities are affected by the preferred orientation due to severe deformation of specimens, Arnell's method was employed to avoid the effect of preferred orientation [8].

Ferrite scope (FS), a product of Fischer Co. Ltd., was also used for measuring volume fraction of α' phase transformed in deformed specimens. The values of $V_{\alpha'}$ were obtained from the arithmetic mean of five FS readings at each lattice point of measurements set in the parallel portion of tensile specimens via the calibration curve depicted in Fig. 2. Figure 2 shows the relationship between α' volume fraction $V_{\alpha'}$ measured by VSM and FS reading, revealing that good linear correlation can be obtained between the two kinds of measured values for a wide range of volume fraction at two levels of temperature, i.e., RT and 77 K.

Figure 3 shows the evolution of volume fraction of α' phase transformed during a tensile test of SUS 304 at RT in air. The value of $V_{\alpha'}$ is increased exponentially with the applied strain level ε in the plastic deformation region as shown by the solid line in Fig. 3. The solid line can be expressed by the following equation:

$$V_{\alpha'} = 100 - \frac{100}{\exp\left[\left\{(\varepsilon + 20.0)/97.9\right\}^{4.0}\right]} \qquad (1)$$

The value of $V_{\alpha'}$ remains small at strain levels lower than 20%, but it reaches as high as 15.5% or higher for ε=43.2 % at RT.

3. Experiments and results

3.1. Fatigue crack propagation tests

Figure 4 shows the geometry of a through-thickness cracked specimen used in the present fatigue crack propagation tests. A crack starter notch was made at the center of each specimen by the electric discharge machining method. The chemical composition of SUS 304 stainless steel is

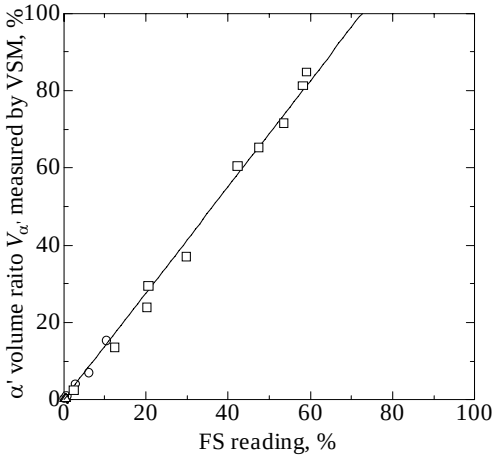

Figure 2*: Calibration curve for for determining values of α' volume fraction $V_{\alpha'}$ by ferrite scope.*

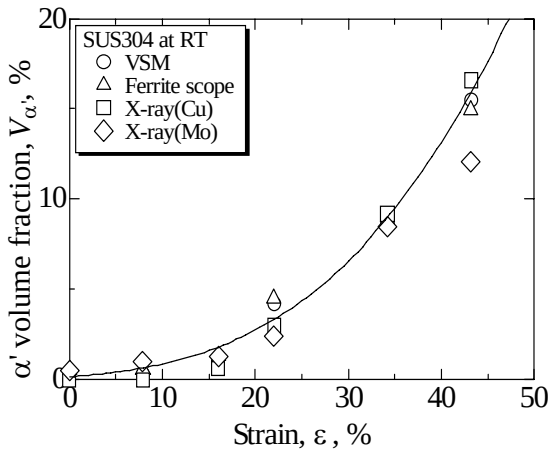

Figure 3*: Plots of α' volume fraction $V_{\alpha'}$ vs. applied nominal tensile strain ε in SUS 304 stainless steel at RT obtained by different measurement methods.*

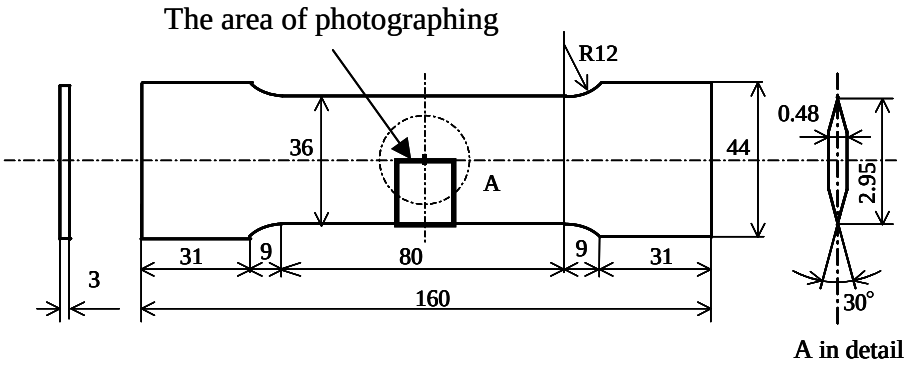

Figure 4*: Geometry of through-thickness cracked specimen (Unit: mm).*

the same as listed in Table 1. Fatigue crack propagation tests were made at maximum stress levels of σ_{max}=202-286 MPa for four levels of stress ratio, i.e., $R=\sigma_{min}/\sigma_{max}$ =0.1-0.4 at RT in air. The tests were intermitted at every crack half length increment of Δa=0.5-1 mm.

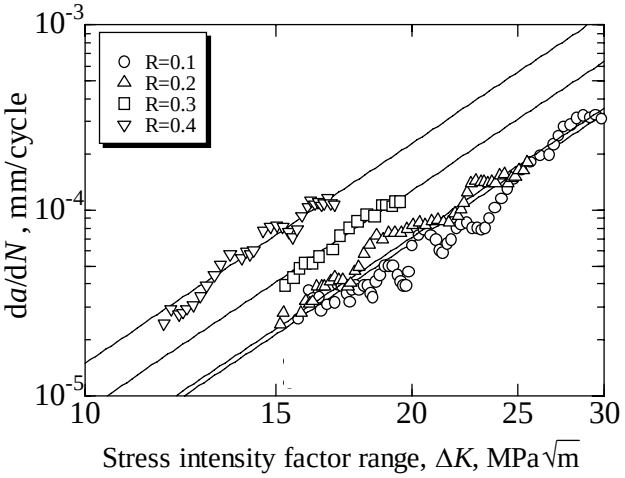

Figure 5*: Comparison of fatigue crack growth behavior in SUS304 steel obtained for different values of the R ratio.*

Figure 5 shows the *R*-dependence of fatigue crack growth behavior in the present SUS 304 steel. The higher the *R* ratio becomes, the higher the crack growth rate becomes. Although the data points fluctuate around the straight lines especially for *R*=0.1 and 0.2, the crack growth rate *da/dN* can be related to the stress intensity factor range $\Delta K=(1-R)K_{max}$ by the following well-known Paris law for all the *R*-ratio values tested:

$$da/dN=C(\Delta K)^m \qquad (2)$$

where *C* and *m* are empirical constants. The value of *m* is obtained as about 4.1 irrespective of the *R* value in the present experiments as shown in Fig. 5. The figure implies that cracks had grown under the stable crack growth condition throughout fatigue crack growth experiments in all the cases investigated in this study.

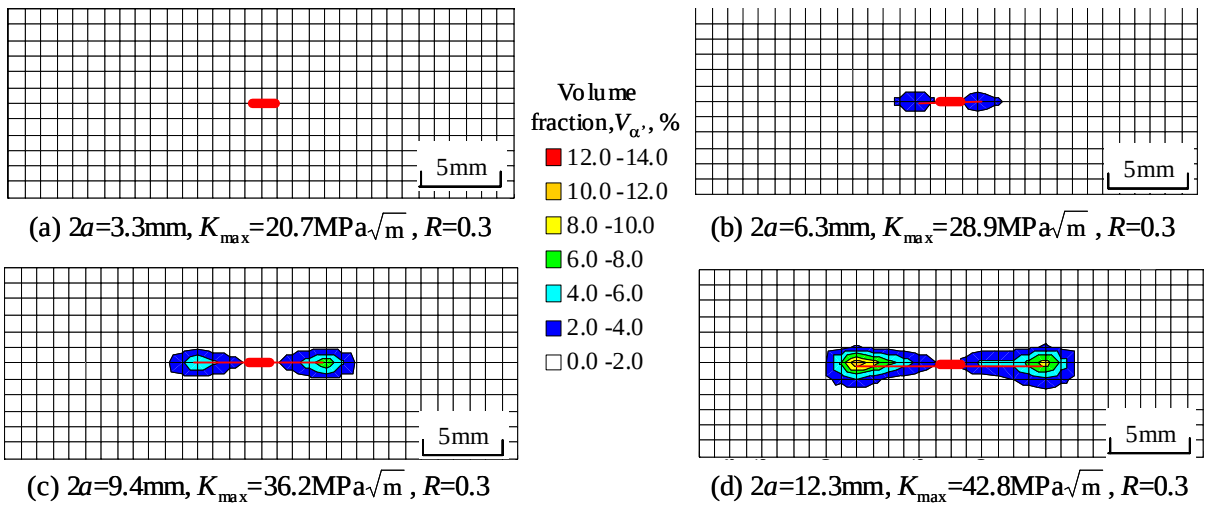

(a) 2*a*=3.3mm, K_{max}=20.7MPa$\sqrt{m}$, *R*=0.3

(b) 2*a*=6.3mm, K_{max}=28.9MPa$\sqrt{m}$, *R*=0.3

(c) 2*a*=9.4mm, K_{max}=36.2MPa$\sqrt{m}$, *R*=0.3

(d) 2*a*=12.3mm, K_{max}=42.8MPa$\sqrt{m}$, *R*=0.3

Figure 6*: Evolution of the spatial distribution of α' volume fraction around a through-thickness fatigue crack in SUS 304 steel measured by ferrite scope where 2a is fatigue crack length, K_{max} the applied maximum stress intensity factor and R the stress ratio.*

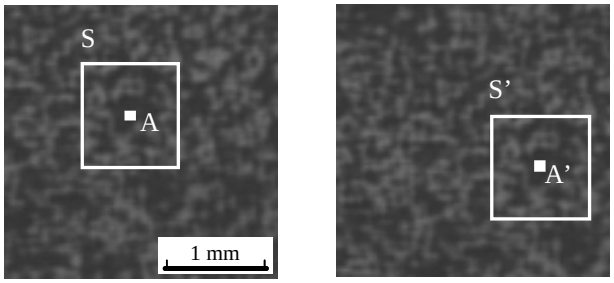

(a) (b)

Figure 7*: Random speckle pattern on the surface of a specimen.*

3.2. Spatial distributions of α' martensitic phase

Ferrite scope was used to obtain spatial distributions of α' volume fraction $V_{\alpha'}$ around fatigue cracks in the present center-cracked specimens. Measurements were made at lattice points having a regular interval of about 1 mm around fatigue cracks and calibrated by the curve shown in Fig. 2. Figures 6(a) trough (d) depict the evolution of the spatial distribution of $V_{\alpha'}$ around a growing fatigue crack in SUS 304 at R=0.4. Austenitic γ phase was transformed into α' phase in the plastic wakes around the tips of the fatigue crack where stress was so high that severe deformation took place. The value of $V_{\alpha'}$ at the crack tip increases as crack length 2a becomes longer and it decreases as the distance from the crack tip becomes longer.

3.3. Strain distributions around fatigue cracks

The digital image correlation (DIC) method was adopted in order to determine strain distributions around fatigue cracks. The DIC method is usually used to measure displacements in deformed specimens by tracking speckle patterns printed on deforming specimens. The method can identify each of the moving points in the speckle patterns by finding similarity of a pattern surrounding it [9].

Figures 7(a) and (b) show CCD camera images of a random speckle pattern sprayed on the surface of a specimen before and after deformation, respectively. An arbitrary point A, the center of a small rectangular area S called a subset in Fig. 7(a), moved to a point A', the center of a subset S' in Fig. 7(b), after deformation. The subsets consist of many pixels having 256 levels of density. If these subsets strongly resemble each other, it is quite possible that the points A and A' in the subsets were the same point and thus the displacement can be obtained as the difference between the points A and A'.

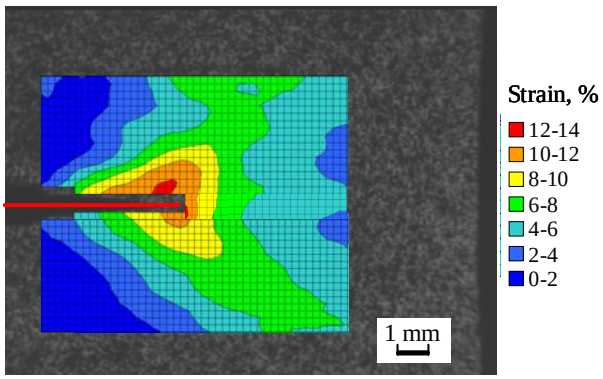

(a) *Strain distribution*

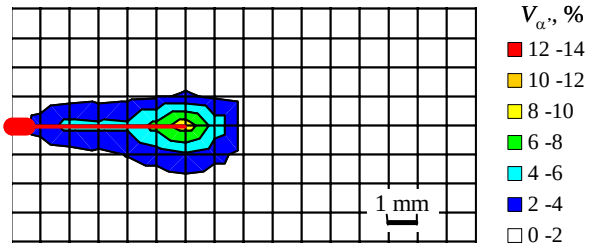

(b) *Contour map of* $V_{\alpha'}$

Figure 8*: Comparison of strain distribution with* $V_{\alpha'}$ *distribution around fatigue crack.*

The x- and y-components of displacement u_i^1 and u_i^2 at an arbitrary point (x_i, y_i) on a specimen surface can be obtained by the moving least-square method from respective displacement components at the neighboring points (i=1, 2, … n). The interpolation function used in the present least squares method is expressed by the following equation (3):

$$\begin{aligned} u_i^I &= u_i^I(x,y) \\ &= a_1^I + a_2^I x_i + a_3^I y_i + a_4^I x_i^2 + a_5^I x_i y_i + a_6^I y_i^2 \\ &(I = 1,2) \end{aligned} \qquad (3)$$

where I=1 and 2 indicate x- and y-components, respectively, and a_J^I (J=1, 2, …, 6) are unknown coefficients to determine. These coefficients can be determined by minimizing the sum of square errors of interpolated and measured displacements. The values of strains at the point (x_i, y_i) can be obtained by the derivatives of Eq. (3).

Figures 8 (a) and (b) compare distributions of $V_{\alpha'}$ and strain around a fatigue crack having a surface length of 2a=12.3 mm at K_{max}= 42.8 MPa$\sqrt{m}$ for R=0.3. Although there exists a blank space along the periphery of a crack in the strain distribution as shown in Fig. 8(a) due to the subset in the DIC calculation, the $V_{\alpha'}$ distribution resembles the strain distribution. The highest values of $V_{\alpha'}$ and strain were always observed near crack tips and found to be correlated well with each other.

3.4. Magnetic flux density distributions around fatigue cracks

Fatigued specimens were at first demagnetized by a demagnetizer that applies AC magnetic field to specimens by gradually reducing the amplitude of the magnetic field to zero. The demagnetized specimens were then magnetized by a high-field DC electromagnet of 0.5 T or higher in the direction of the *x*-axis, i.e., in the direction parallel to fatigue cracks. A magnetic field of 0.4 T induced by electro-magnet is considered sufficient to put fatigued specimens in saturation magnetization states. After the magnetization, the magnetic flux leakage was measured by scanning a flux gate sensor above fatigue cracks with a lift-off of 3 mm. The measurements were automatically made on the front and back surface sides of the specimens by the use of a computer-controlled *x*-*y* table at grid points of 1 mm by 1mm in rectangular regions of 23 mm in the longitudinal direction by 37 mm in the width direction of the specimens with cracks placed at the center of the measurement regions.

Figure 9 shows a 3-D distribution of vertical magnetic flux density B_z above a fatigue crack having a surface length of $2a$=14.4 mm at K_{max}= 36.7 MPa$\sqrt{m}$ for R=0.4. The vertical magnetic flux density B_z here means the component of leakage magnetic flux **B** normal to specimen surface. The minimum negative peak was observed above the left crack tip near the north pole of the electromagnet, whereas the maximum positive one above the right crack tip near the south pole of the magnet. As indicated in Fig. 9, leakage magnetic flux density reflects the distribution of the volume fraction of α' martensite transformed in the wakes around the two fatigue crack tips so that the distance $2l$ between the outermost minimum and maximum peaks for the *x*-direction magnetization can be correlated with real crack length $2a$. Figure 10 shows the relations between real crack length $2a$ and the distance $2l$ for different R values tested. All the data points in Fig. 10 can be expressed well by a single straight line irrespective of the R value, implying that the measurement of $2l$ can estimate real crack length $2a$ in a fatigued specimen. The inclination of the line in Fig. 10 is 0.84, i.e., smaller than unity, indicating that estimated crack length is always larger than real one for the *x*-direction magnetization. A diagram like Fig. 10 can make a conservative estimation of real crack length in, say, in-service inspection of a cracked component of a structure.

The magnitude of the peaks changes according to

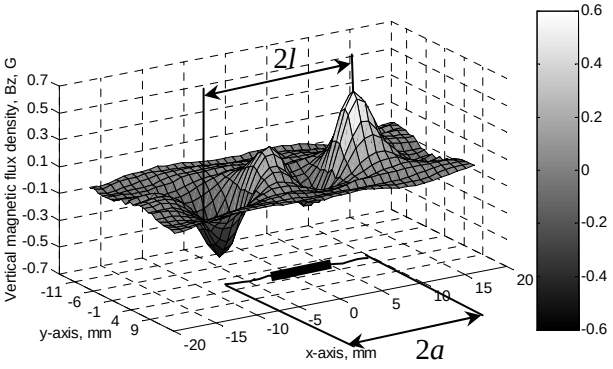

Figure 9*: 3-D distribution of the vertical magnetic flux density B_z above a fatigue crack of 2a=14.4 mm at K_{max}= 36.7 MPa$\sqrt{m}$ for R=0.4 in a SUS 304 steel plate specimen magnetized in the x-axis direction.*

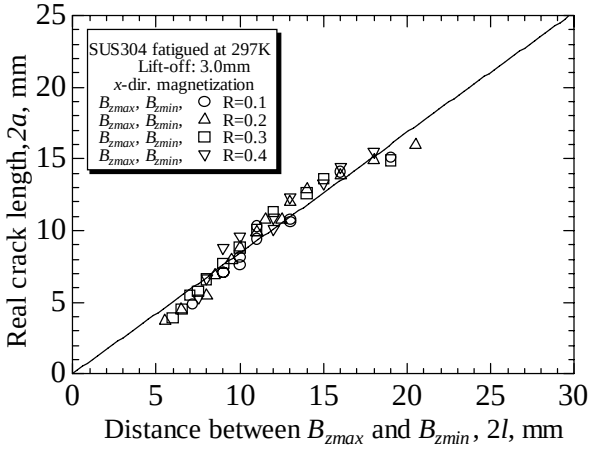

Figure 10*: Real crack length 2a as a function of the distance 2l between the maximum and minimum peaks of the vertical leakage magnetic flux density distribution B_z above fatigue cracks in SUS304 plates.*

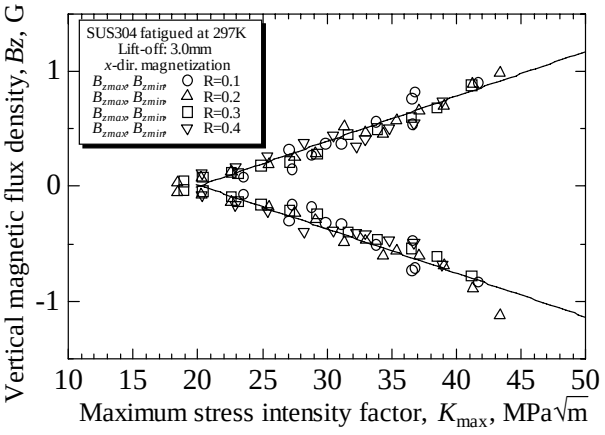

Figure 11*: Maximum peak value B_{zmax} and minimum peak value B_{zmin} of vertical leakage magnetic flux density B_z vs. applied maximum stress intensity factor K_{max} relations.*

the fatigue damage specimens have suffered, or the volume of plasticity-induced martensitic phase transformed in plastic wake regions around fatigue cracks. Figure 11 shows the B_{zmax} vs. K_{max} and the B_{zmin} vs. K_{max} relations obtained by experiments. Each relation can be represented by one single straight line irrespective of R-ratio. This result implies that the damage introduced in the plastic wake regions around a fatigue crack is controlled by the value of the applied maximum stress intensity factor K_{max}. The solid lines in Fig. 11 indicate that the measurement of the maximum and/or minimum leakage magnetic flux density can estimate the value of the applied K_{max} or that of the applied maximum stress level σ_{max} a structural component of SUS 304 may have been subjected to in service.

4. Conclusions

In this study, we have attempted to establish a new non-destructive method not only for estimating crack length but for quantitatively evaluating the maximum value of stress intensity factor applied in an austenitic stainless steel SUS304 (equivalent of AISI304) fatigued at RT in air.

The method makes use of plasticity-induced martensitic phase transformation that takes place in the plasticity wake regions around growing fatigue cracks. Distributions of the volume fraction of α' martensitic phase $V_{\alpha'}$ around fatigue cracks were measured with ferrite scope. The results were compared with the distributions of strain measured by the digital image correlation (DIC) method and with those of vertical magnetic flux density B_z above the fatigue cracks in plate specimens magnetized by a strong electromagnet. The maximum values of $V_{\alpha'}$ and the peak values of B_z (B_{zmax} and B_{zmin}) were observed at the vicinity of the crack tip where the maximum values of strain were measured by the DIC method. The maximum values of $V_{\alpha'}$ and the peak values of B_z around fatigue cracks were increased with an increase of the maximum value of strain measured. It was also revealed that the B_z distributions above the cracks reflected the α' phase distributions in the plastic wake regions produced around the cracks; i.e., the distance between the points where B_z reached the maximum and the minimum values B_{zmax} and B_{zmin} had linear correlations with crack length $2a$. The B_{zmax} and the B_{zmin} values also showed good linear relations with maximum stress intensity factors K_{max}. These results imply that not only crack length but also maximum values of the applied stress intensity factor can be quantitatively evaluated in an electromagnetic non-destructive way.

5. References

[1] Nishiyama, Z., "*Martensitic Transformation*," Academic Press, 1978.

[2] Reed, R. P. and Gunter, C. J., "Stress-Induced Martensitic Transformations in 18Cr-8Ni Steel," *TMA-AIME*, Vol. 230: 1713-1718, 1964.

[3] Angel, T., "Formation of Martensite in Austenitic Stainless Steels: Effects of Deformation, Temperature, and Composition," *J. Iron and Steel Inst.*, Vol. 177: 165-174, 1954.

[4] Menard, J. and Weil, L., *Advances in Cryogenic Engineering*, Vol. 6: 587-589, 1960.

[5] Nakasone, Y. and *et al*., Report of Research Committee on the Application of Electromagnetic Fracture Mechanics to the NDE of Damage and Degradation, JSAEM- R-9803, 9903 and 0005 (in Japanese), 1999, 2000 and 2001.

[6] Nakasone, Y. and *et al*., *Mesomechanics of Computation and Design of Use-Specific Materials* (G. C. Sih, et. al. eds.): 192-197, 2003.

[7] Nakasone, Y. and *et al*., *IUTAM symposium on Mesoscopic Dynamics of Fracture Process and Materials Strength (H. Kitagawa and Y. Shibutani eds.),* Kluwer Academic Publishers: 321-330, 2003.

[8] Arnell, R. D., "*Determination of Retained Austenite in Steel by X-ray Diffraction*," *J. Iron and Steel Inst*., Vol. 206: 1035- 1036, 1968.

[9] Yoneyama, S. and Morimoto, Y., "*Accurate Displacement Measurement by Correlation of Colored Random Patterns*," *JSME Int. J*., Ser. A, Vol. 46:178-184, 2003.